Received: 27 April 2023 | Revised: 23 August 2023 | Accepted: 21 September 2023

DOI: 10.1002/mrm.29885

Magnetic Resonance in Medicine

TECHNICAL NOTE

Real-time water/fat imaging at 0.55T with spiral out-in-out-in sampling

Ye Tian[1] | **Krishna S. Nayak**[1,2]

[1]Ming Hsieh Department of Electrical and Computer Engineering, Viterbi School of Engineering, University of Southern California, Los Angeles, California, USA

[2]Department of Biomedical Engineering, Viterbi School of Engineering, University of Southern California, Los Angeles, California, USA

Correspondence
Ye Tian, Ming Hsieh Department of Electrical and Computer Engineering, Viterbi School of Engineering, University of Southern California, 3740 McClintock Ave, EEB 406, Los Angeles, CA 90089-2564, USA.
Email: ytian607@usc.edu

Funding information
National Institutes of Health, Grant/Award Numbers: R01-HL130494, R21-HL159533; National Science Foundation, Grant/Award Number: 1828736; American Heart Association, Grant/Award Number: 903839

Abstract

Purpose: To develop an efficient and flexible water/fat separated real-time MRI (RT-MRI) method using spiral out-in-out-in (OIOI) sampling and balanced SSFP (bSSFP) at 0.55T.

Methods: A bSSFP sequence with golden-angle spiral OIOI readout was developed, capturing three echoes to allow water/fat separation. A low-latency reconstruction that combines all echoes was available for online visualization. An offline reconstruction provided water and fat RT-MRI in two steps: (1) image reconstruction with spatiotemporally constrained reconstruction (STCR) and (2) water/fat separation with hierarchical iterative decomposition of water and fat with echo asymmetry and least-squares estimation (HIDEAL). In healthy volunteers, spiral OIOI was acquired in the wrist during a radial-to-ulnar deviation maneuver, in the heart without breath-hold and cardiac gating, and in the lower abdomen during free-breathing for visualizing small bowel motility.

Results: We demonstrate successful water/fat separated RT-MRI for all tested applications. In the wrist, resulting images provided clear depiction of ligament gaps and their interactions during the radial-to-ulnar deviation maneuver. In the heart, water/fat RT-MRI depicted epicardial fat, provided improved delineation of epicardial coronary arteries, and provided high blood-myocardial contrast for ventricular function assessment. In the abdomen, water-only RT-MRI captured small bowel mobility clearly with improved water-fat contrast.

Conclusions: We have demonstrated a novel and flexible bSSFP spiral OIOI sequence at 0.55T that can provide water/fat separated RT-MRI with a variety of application-specific temporal resolution and spatial resolution requirements.

KEYWORDS

0.55 Tesla, real-time MRI, spiral out-in-out-in, water/fat separation

A preliminary version of this work was presented at ISMRM 2022, Abstract #317 (oral presentation).

1 | INTRODUCTION

Real-time MRI (RT-MRI) has the unique ability to reveal organ movements and interactions as they occur in a non-invasive, radiation-free fashion, without requiring any repetition or invoking any assumption of periodic motion. RT-MRI provides valuable diagnostic information in areas that undergo irregular motion, such as the heart, joints, abdomen, and vocal tract,[1] and enables the guidance of interventions where it is necessary to visualize the dynamic anatomy and the interventional instruments.[2] Recently, RT-MRI on 0.55T MRI systems with high-performance gradients have shown promising results by leveraging efficient spiral trajectories and bSSFP imaging.[3,4] Such systems are favorable for RT-MRI due to reduced specific absorption rate (SAR), reduced susceptibility at air-tissue interfaces, shorter T_1 and longer T_2*, which together allow for more flexible pulse sequence design, and higher acquisition efficiency[5] compared to conventional field strengths.

Many RT-MRI regions of interest could benefit from water-fat separation. In the heart, RT-MRI is often used to capture cardiac mechanics, characterize intracardiac flow, and localize coronary arteries. The myocardium and blood of the heart are mostly water, and pericardial and epicardial fat is also present, surrounding the heart and coronary arteries. Fat suppression improves the depiction of coronary arteries and the epicardial contour. In the musculoskeletal system, RT-MRI is used to capture joint movement, instability, and restrictions.[6] Bone marrow contains both fat and water, while the other tissues such as synovial fluid, ligaments, tendons, and cartilage are primarily water. Fat or water suppression techniques improve visualization of the underlying musculoskeletal dynamics.[7] In the abdomen, RT-MRI can be used to assess small bowel motility. Fat suppression significantly improves the contrast between the small bowel and adjacent visceral adipose tissue.[8–10]

Several MRI techniques have been developed to achieve water- or fat-only imaging or water/fat separated imaging. At 1.5T or 3T, it is common to use spectral-spatial excitation pulses[11] to select one component. However, due to the reduced water and fat resonance frequency difference at 0.55T ($\Delta f = 80$ Hz), it would require a very long RF excitation pulses (~18 ms) to achieve a comparable frequency selection.[12] Another approach uses preparation pulses such as spectrally-selective saturation pulse or inversion recovery pulse to suppress one component[13]; however, these preparation pulses are sensitive to B_0 inhomogeneities, can be insufficient due to a shorter T_1 of fat, and less flexible in image contrast. Preparation pulses also interrupt the steady-state, can introduce transient artifacts, and reduce scan efficiency, making them less favorable for RT-MRI.

In this work, we perform water/fat separated imaging by acquiring multiple echoes per TR and employing chemical-shift-based separation.[14–20] We utilize a novel spiral out-in-out-in (OIOI) trajectory that leverages the reduced off-resonance and contemporary gradient performance at 0.55T. This trajectory provides four image series at three TEs, enabling water/fat separation. We demonstrate application to the wrist during voluntary movements designed to test joint stability, the heart during free breathing and without cardiac gating, and the small bowel during normal gastrointestinal motion.

2 | METHODS

2.1 | Spiral OIOI trajectory design

Figure 1 illustrates the pulse sequence and the spiral OIOI trajectory used in the heart application. The variable density spiral-out trajectory was designed[21] with a maximum slew rate of 175 mT/m/ms and a maximum gradient strength of 23.7 mT/m. Spiral out-in was then formed by concatenating the spiral-out with its time-reversed spiral-in. Note that the spiral-out tail must be modified to achieve a smooth transition between the spiral-out and spiral-in, where we slowed down the gradient along the radial direction to zero (with 175 mT/m/ms slew rate) and maintained the gradient in the circumferential direction. This impacted a small portion of the gradient waveform (11.58%) and permitted a high acquisition efficiency. Two spiral out-in trajectories are combined with a 180° relative rotation to form spiral OIOI.

With a single spiral being 2.034 ms, the spiral OIOI has a total readout duration of 8.136 ms. The TEs were 0.96, 4.99, and 9.06 ms. The echo spacing is such that the water/fat chemical shift is approximately $2\pi/3$ phase difference between adjacent echoes[22]: $\Delta TE = 1/(3 \times \Delta f)$.[23] The spiral OIOI trajectory has zero M_0 and M_1 moments at the three TEs as shown in Figure 1C, which can reduce artifacts from in-plane constant speed flow.[24] Table S1 contains detailed parameters for the three applications.

During RT-MRI acquisition, each spiral OIOI trajectory is rotated with golden angle (111.25°) after each TR, which benefits constrained reconstruction[25] and allows for flexible selection of the reconstruction FOV and temporal resolution.[26,27] Reconstruction FOV was selected to include all signal area to avoid spiral aliasing artifact.[28] We report both the FOV during the single spiral-out trajectory design and the FOV used for image reconstruction in Table S1.

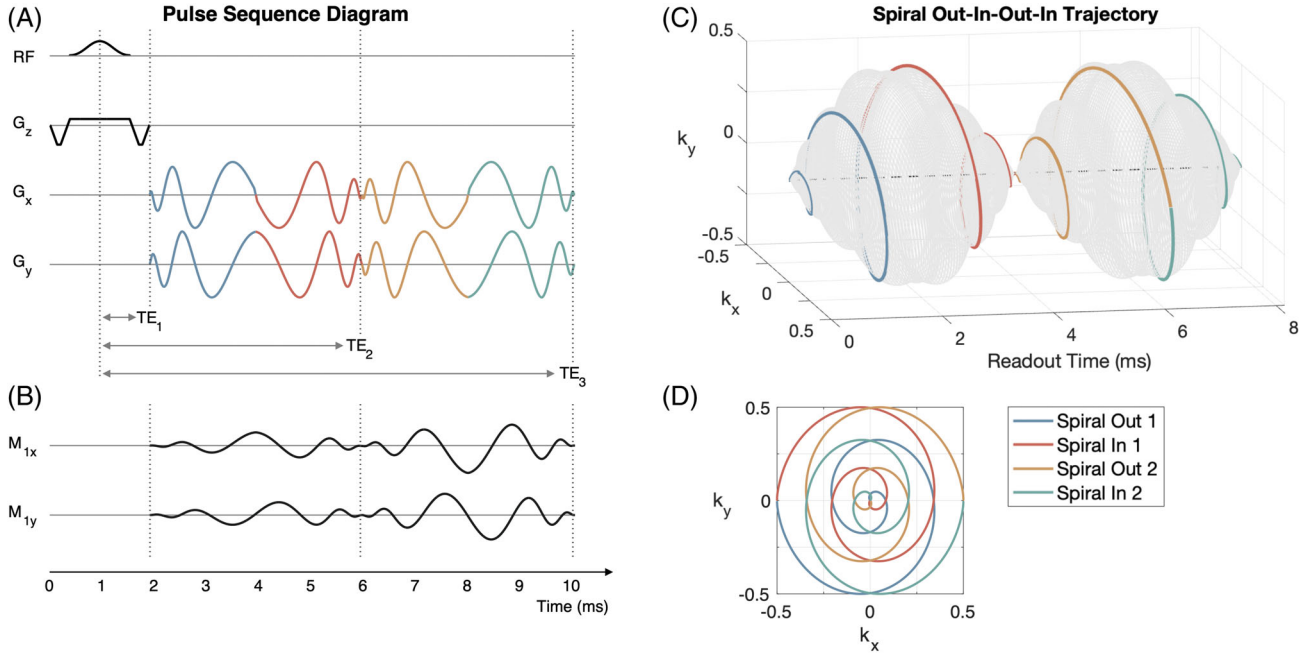

FIGURE 1 Pulse sequence diagram and k-space trajectory for spiral OIOI RT-MRI. (A) The pulse sequence is bSSFP with spiral OIOI readout. Four spirals have effective TEs (k_x, $k_y = 0, 0$) at $t = 0.96$ ms, 4.99 ms, 4.99 ms, and 9.06 ms, respectively. For each spiral out-in, both the M_0 (zeroth moment, not shown) and M_1 (first moment, shown in (B)) are nulled at the TEs, making the sequence robust to motion and flow artifacts. The readout trajectory is illustrated in (C) k_x-k_y-t_r space (where t_r is the time from the start of the readout) and in the (D) k_x-k_y plane.

2.2 | Online reconstruction

Online image reconstruction was implemented in the RTHawk real-time system[29] (HeartVista Inc. Los Altos, California), which is a gridding reconstruction using data from all echoes. This reconstruction used a pre-defined temporal resolution and FOV as listed in Table S1 and was used to ensure correct slice positioning, and a rough water-only or fat-only image depending on the center frequency. Effective oversampling factor (or effective undersampling factor, as reported later in *Offline Reconstruction*) is reported in Table S1, defined as the total number of spiral OIOI interleaves divided by the number of uniformly sampled spiral interleaves needed to achieve the desired unaliased FOV. Note that the oversampling/undersampling factor is a function of reconstructed FOV due to the use of golden-angle sampling.[27]

2.3 | Offline reconstruction

Offline image reconstruction was performed with the water/fat separation pipeline shown in Figure 2. The two-step reconstruction includes RT image reconstruction of each image series with spatiotemporally constrained reconstruction (STCR)[30] followed by concomitant field phase correction and water/fat separation with HIDEAL.[14]

Offline reconstruction was implemented in MATLAB 2021a (MathWorks, Natick, Massachusetts) and on a server equipped with 4x AMD EPYC 7502 32-Core CPU, 504 Gb CPU memory, and 4x NVIDIA A100 GPU with 40 Gb memory on each core.

2.3.1 | Constrained reconstruction

K-space trajectory was predicted by gradient impulse response function prior to reconstruction.[31] Four image series corresponding to each of the spiral arms in spiral OIOI were reconstructed separately by STCR[30] with the same regularization parameters. Sensitivity maps were estimated from temporally averaged first spiral-out data using the Walsh method.[32] The FOV during iterative reconstruction was kept large enough to include all areas that have signal to avoid aliasing,[28] as reported in Table S1.

Temporal resolution and regularization parameters were selected through a parameter sweep. The temporal resolution was selected to balance the imaging artifact and motion blurring separately for each application as reported in Table S1. Figure S1 shows representative temporal resolution sweep results from one cardiac dataset. Reconstruction regularization parameters were manually selected so that the image has minimal spatial and temporal blurring as well as the least amount of

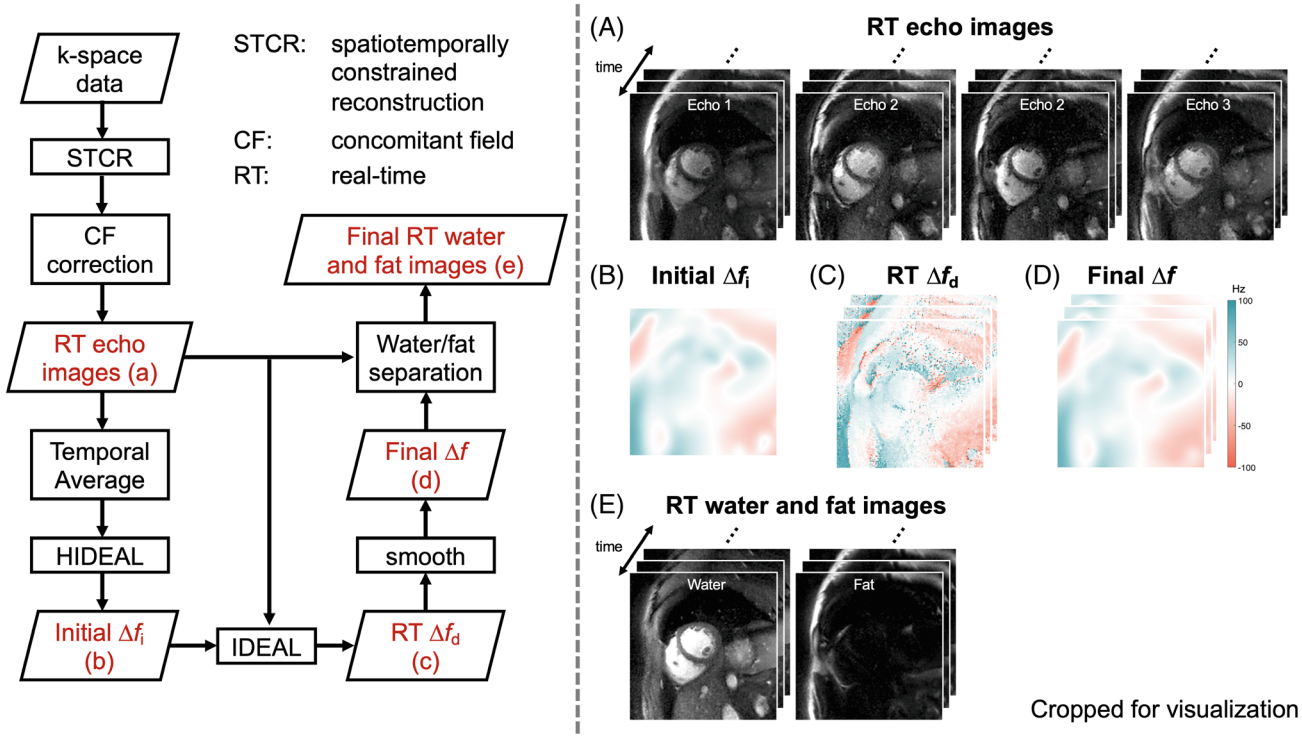

FIGURE 2 Offline water/fat separated reconstruction pipeline. The reconstruction pipeline is shown on the left, and selected intermediate results are displayed on the right. The acquired k-space data are reconstructed by STCR and followed by concomitant field phase (CF) correction to obtain (A) four RT images, one representing each readout segment. Hierarchical IDEAL is applied to the temporally averaged image series to obtain (B) an initial off-resonance map Δf_i. IDEAL is then performed for each time frame, using Δf_i as the initial guess for the RT off-resonance map. This results in (C) a dynamic off-resonance map Δf_d that is smoothed to produce (D) a final off-resonance map Δf that is used for water/fat separation, producing (E) RT water/fat images.

artifact. Specifically, the STCR regularization parameters were: $\lambda_t = 0.01\ C$ and $\lambda_s = 0.001\ C$, where C represents the highest pixel intensity in the coil-combined gridding reconstruction.

2.3.2 | Concomitant field effects correction

To first-order approximation, concomitant field effects are proportional to $1/B_0$ and G^2; thus, they are an important consideration when using high-gradient performance low field systems.[33] The concomitant fields result in a phase accumulation over time that is spatial location dependent and can cause image distortion and banding artifact. This phase accumulation, if not corrected, can lead to water/fat swaps. We applied the multi-frequency interpolation (MFI) method[34] on STCR reconstructed images to correct for the concomitant field phase, with a frequency bin of 1 Hz and ≤300 bins for a FOV of 56 × 56 cm^2. Figure S2 compares the water/fat separation results and estimated off-resonance maps with and without concomitant field phase correction.

2.3.3 | Water/fat separation

Water/fat separation utilized a customized hierarchical iterative decomposition of water and fat with echo asymmetry and least-squares estimation (HIDEAL).[14] First, low-resolution images were generated from the RT image series, with 2× time coarser for each level until reaching approximately 25 × 25 mm^2. A region-growing IDEAL[15] was applied on the lowest resolution image to obtain an initial off-resonance map. The process continues at higher levels, taking interpolated off-resonance maps from lower levels as initial estimates and utilizing pixel-independent IDEAL for refining the off-resonance map, until the original resolution was achieved. HIDEAL was performed on the temporally averaged images first, and the resulted off-resonance map was used as an initial estimation for IDEAL processing on each individual time frame. A median filter of size [7] in [x, y, t] was applied on the resulted dynamic off-resonance map. Finally, dynamic off-resonance map was smoothed by a filter as used in Tan et al[17]:

$$T = \mathcal{F}^{-1}(1 + w \cdot \|\vec{k}\|)^{-h}$$

with parameters $w = 64$ and $h = 8$, where $\mathcal{F}^{-1}$ represents the inverse Fourier transform and $\vec{k}$ is a 2D grid matrix ranging from −0.5 to 0.5. The smoothed off-resonance map was used to generate final water/fat separated RT images.

2.4 | Experiments

Experiments were performed on a whole-body 0.55T system (prototype Magnetom Aera XQ, Siemens Healthineers, Erlangen, Germany) equipped with high-performance shielded gradients (45 mT/m amplitude, 200 T/m/s slew rate). Imaging was performed with RTHawk real-time system (Vista.ai, Palo Alto, CA).[29] The study was approved by the Institutional Review Board of the University of Southern California. All volunteers provided written informed consent. The scan parameters were tailored to each application and are summarized in Table S1, with references from previous publications of RT-MRI of the heart,[12] wrist,[35,36] and abdomen.[8,37]

2.4.1 | Wrist scans

Five volunteers (two female, three male, age 31 ± 8 y) were imaged in a squatting or kneeling position at the back of the scanner, with the right hand (imaging hand) placed at the magnet isocenter between two body-6 arrays (one posterior and one anterior). The upper body-6 array was supported by sandbags, leaving a space for the wrist to move. RT-MRI was acquired for ∼15 s when performing a radial-to-ulnar deviation maneuver, which is relevant to evaluation for dynamic scapholunate instability.[35] Before imaging, water bottles were placed around the hand as needed to ensure sufficient signal for the scanner to calibrate the center frequency of water. Then center frequency was tuned for imaging fat. ROI shimming was performed over the base of the wrist and covering all relevant bones and ligaments of the wrist. Imaging parameters: voxel size 1.1 × 1.1 × 6 mm^3, TR 10.8 ms, TEs 0.6/4.6/8.7 ms, reconstruction undersampling factor 12.3, reconstruction temporal resolution 108 ms/frame.

2.4.2 | Cardiac scans

Five volunteers (three female, two male, age 29 ± 4 y, resting heart rate 65 ± 9 beats/min) were scanned during free breathing and without cardiac triggering. Data were collected with the body-6 array (anterior) and six elements from spine array. In each volunteer, a short-axis slice of mid-ventricular myocardium, a four-chamber slice, and a two-chamber long-axis slice were acquired for 15 s each. ROI shimming was performed for the ventricles and excluding the chest wall. Imaging parameters: voxel size 1.5 × 1.5 × 8 mm^3, TR 10 ms, TEs 1/5/9 ms, reconstruction undersampling factor 19.8, reconstruction temporal resolution 40 ms/frame.

2.4.3 | Abdomen scans

Three volunteers (one female, two male, age 31 ± 14 y) were scanned to visualize small bowel motility. Subjects were instructed to drink one liter of neutral MRI contrast agent (Breeza, Beekley Medical, Bristol, Connecticut) gradually within 45–60 min before the scan to expand and enhance the signal in the small bowel. Data were collected with the body-6 array (anterior) and six elements of the spine array. Ten to 12 coronal slices were acquired during free breathing, covering the entire small bowel (15 s per slice). Imaging parameters: voxel size 2.4 × 2.4 × 10 mm^3, TR 10.3 ms, TEs 1.1/5.2/9.3 ms, reconstruction undersampling factor 4.4, reconstruction temporal resolution 165 ms/frame.

3 | RESULTS

Figure 3 illustrates the results of online and offline reconstructions for the wrist scan during radial-to-ulnar deviation maneuver and Video S1 shows the corresponding video. The online reconstruction had a temporal resolution of 744.5 ms/frame, circular FOV with 14 cm diameter, and used data from all echoes, providing a rough fat-only image. This online reconstruction has low latency (<200 ms)[38] and was adequate for ensuring the correct scan plane, verifying adequate shimming, and performing cursory inspection of artifacts.

The offline reconstruction required a computational time of 8.60 s/frame, providing separate water and fat component movies, and effective separation, even in areas with significant off-resonance (green arrows). Offline reconstruction also provides movies with high temporal resolution at 107.9 ms/frame with reduced motion blurring (orange arrows). Bone marrow, with its substantial fat content, appears bright in the fat-only image; and synovial fluid appears most clearly in the water-only image. The scapholunate ligament gaps and their interactions are clearly visualized during motion on both water (bright) and fat (dark) images. Offline reconstructions for all subjects are shown in Video S2.

Figure 4 shows the four-chamber cardiac water/fat images for all five cardiac volunteers, and the corresponding videos are provided in Video S3. The sequence achieved consistent successful RT water/fat separated

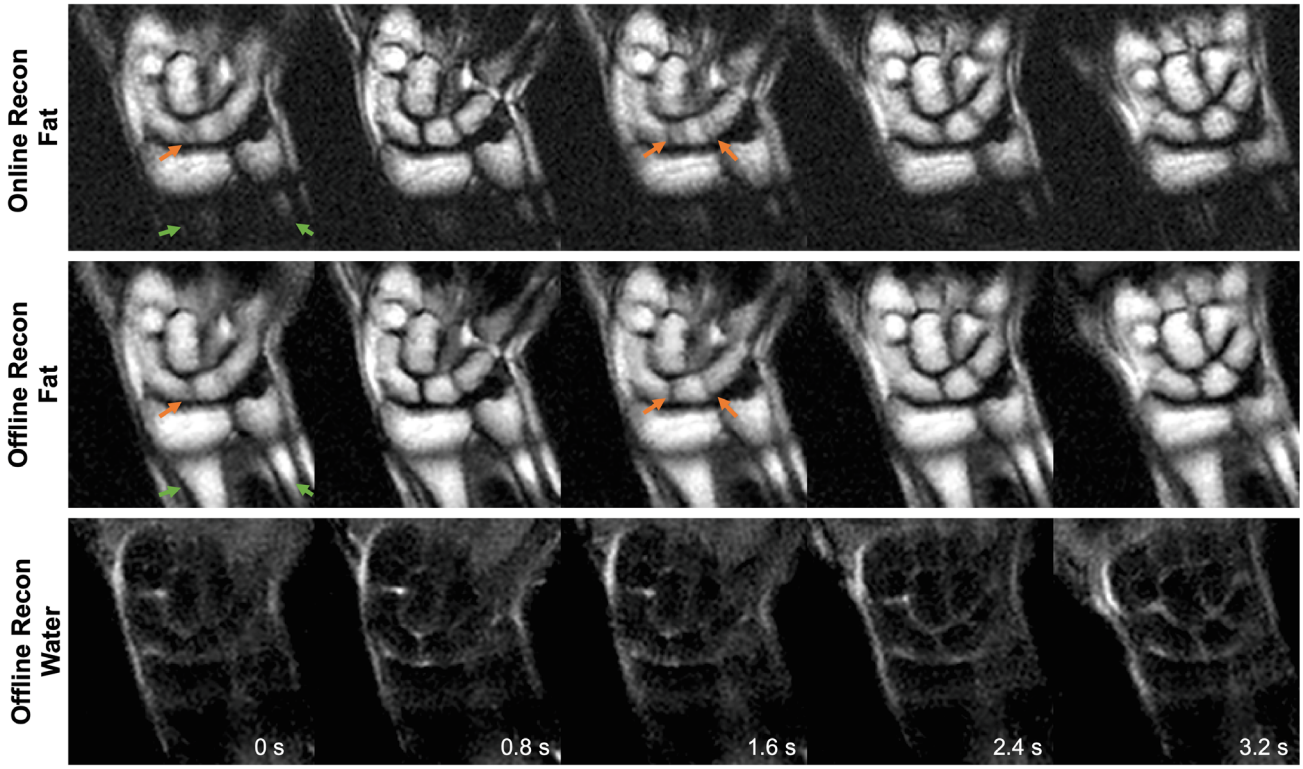

FIGURE 3 Illustration of (top) online low-latency reconstruction and (mid and bottom) offline reconstruction of the moving wrist. The volunteer was performing a radial-to-ulnar deviation maneuver, which is important in the evaluation of dynamic wrist instability. The online reconstruction is a gridding reconstruction that superimposes all of the samples, and gives a rough fat-only or water-only image depending on the center frequency (fat-only in this example). Online reconstruction provides low-latency (<200 ms) and coarse temporal resolution (1.3 frames/s). The offline reconstruction provides water and fat images with high temporal resolution (9.3 frames/s) that has minimal temporal blurring (orange arrows). Offline reconstruction is also insensitive to B_0 inhomogeneity, concomitant field phase, or the combination of both (green arrows). Corresponding video can be found in Video S1.

images across all subjects. The water/fat images captured the detailed structures such as the right coronary artery and left circumflex artery as pointed in Figure 4 by blue arrows and orange arrows, respectively. We do notice a higher flow artifact in volunteer 4, which is likely due to the long readout time. Water/fat separation can fail when large flow appears, but it is easily readthrough and generally does not affect visualization of more static tissues such as the epicardial fat.

Figure 5 shows a representative image of the abdomen scan, and the corresponding video is provided in Video S4. The small intestine, which was filled by Breeza, appears bright on the water-only image, providing a clear depiction of the anatomy and small bowel motility. The green arrows in Figure 5 point clear movements of the small intestine. Note that these images were acquired during free breathing, which will induce a bulk respiratory motion of the organs, which can be read though and distinguished from small bowel movements. Results from all subjects are shown in Video S5.

4 | DISCUSSION

We have developed a spiral OIOI bSSFP pulse sequence and spatiotemporally constrained reconstruction followed by HIDEAL for water/fat separated RT-MRI at 0.55T. This imaging method can be easily adapted to the spatial and temporal resolution requirements of different applications, and was successfully demonstrated in the heart, wrist, and abdomen.

The proposed method effectively provides high temporal resolution water- and fat-only RT images for dynamic visualization of the region of interest. Magnetization prepared Cartesian bSSFP, available on most commercial scanners, can also offer dynamic MRI with water- or fat-only contrast. However, this approach typically yields a low temporal resolution (~400 ms/frame) due to less efficient Cartesian sampling and frequent application of the spectral selective saturation pulse for magnetization preparation. The fat suppression pulse is suboptimal at 0.55T without optimization. This is

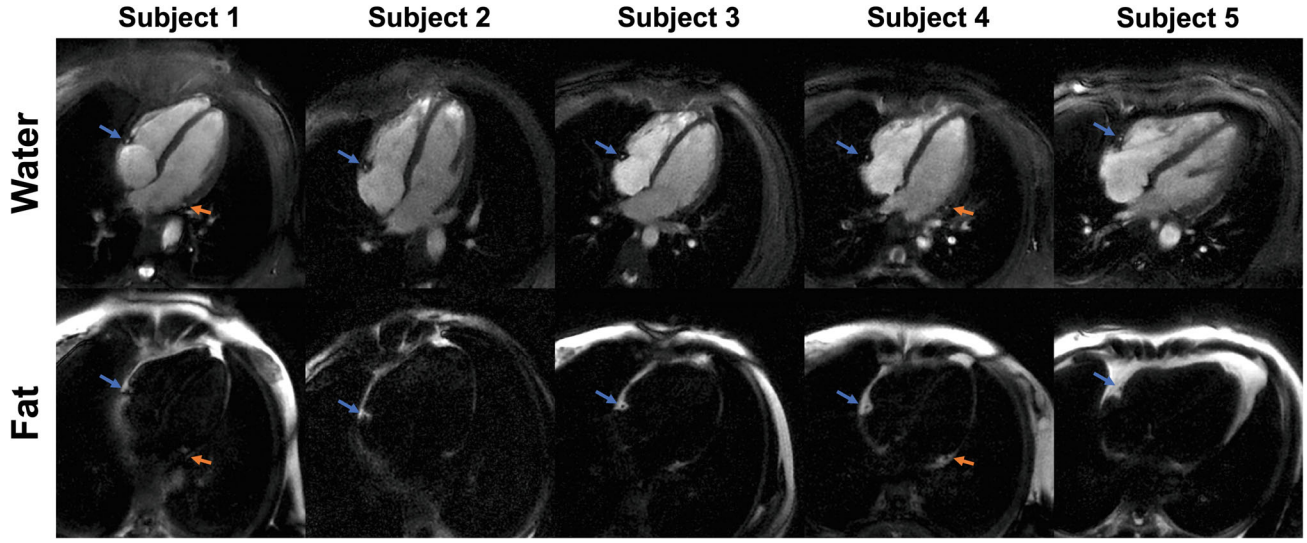

FIGURE 4 Water/fat separated cardiac RT-MRI. One representative time frame from a four-chamber view is shown from five volunteers. Water/fat images obtained by spiral OIOI offer clear epicardial fat depiction and reveal detailed structure. The right coronary artery (blue arrows) and left circumflex artery (orange arrows) are clearly seen in cross-section from the water images. The surrounding fat is also clearly visible in the fat images. Corresponding video showing one cardiac cycle from RT series is provided in Video S3, where we notice some artifacts in the blood pool and aorta, likely due to phase from in-plane flow.

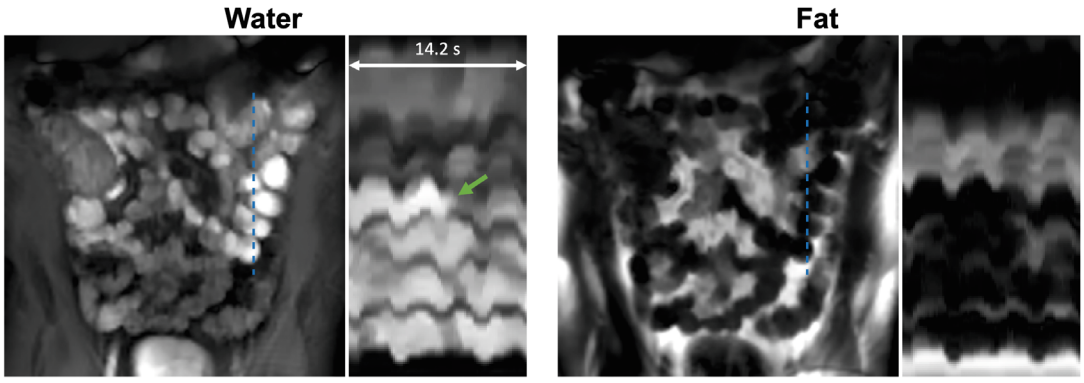

FIGURE 5 Water/fat separated small bowel RT-MRI. Images and intensity vs. time plots are shown for one subject during free breathing, after drinking Breeza GI contrast agent. The intensity vs. time profiles matches the blue dashed line. The water only image provides a clear depiction of the small bowel without the often-confounding presence of visceral adipose tissue signal. Small bowel motility can be evaluated during normal respiration (green arrow). We did observe artifacts on both water image and fat images, which is likely caused by residual gas bubbles, which can occur when subjects do not comply with the contrast agent consumption protocol. Corresponding video is provided in Video S4.

demonstrated by comparing RT Cartesian image with and without fat-suppression and spiral OIOI in Figure S3. The spiral OIOI method achieves excellent water of fat suppression compared with the first spiral-out image (which is a water and fat in-phase image), as shown in Figure S4. Further details of these comparisons are provided in Supporting Information: Additional Experiments. Cartesian DIXON method[39] can be utilized when temporal resolution requirement is relaxed, however, spiral methods generally provide improved efficiency.[40]

This study focused on qualitative water/fat separation, which is of great use when fat or water suppression provides improved depiction/conspicuity of key features that are undergoing motion. This includes the coronary artery lumen, which is surrounded by epicardial fat, or bowels, which are surrounded by visceral fat. Wrist ligament gaps also have better conspicuity in either water-only or fat-only movies. Quantitative water/fat separation is an appropriate next step and may enable better measurement of proton density fat fraction in moving structures.

This would benefit from model-based reconstruction,[17] the use of multipeak fat models,[23] and will likely require added consideration of the bSSFP signal profile across resonance frequencies.

This work utilized a spiral OIOI trajectory, a combination of four spirals to achieve three TEs within each TR, which gave a high readout efficiency and a duty cycle (T_{read}/TR) of ~81% (typical duty cycle for bSSFP at 1.5T and 3T is ~35%). Other readout trajectories are possible, such as rosette, multi-echo spiral-out, or multi-echo radial. Spiral trajectory with self-retracing was also used to minimize off-resonance blurring.[41,42] The spiral OIOI trajectory has superior efficiency since there is no need to slow down the entire gradient during transitions.[43] Off-resonance blurring is also minimal in the offline reconstructed images. This is because the off-resonance induced blurring in spiral imaging is related to the accumulated off-resonance phase over each readout period. This study used a short spiral ~2.04 ms and the estimated off-resonance within the ROI was typically within ±20 Hz, leading to sub-pixel blurring. When the approach is extended to a larger FOV or 3D imaging such as stack-of-spiral[44,45] or spiral OIOI projection,[46] concomitant field effects, off-resonance, and gradient nonlinearity will be of greater concern, and may require model-based reconstruction to fully resolve.[33]

In diagnostic RT-MRI, it is common to utilize a low-latency online reconstruction to ensure slice positioning and adequate image quality, and a more accurate high-latency offline reconstruction for final images. There may be scenarios, such as during image guided interventions, where a high-quality low-latency reconstruction is needed. A limitation of this work is that the offline reconstruction is computationally intense. Compared with the online reconstruction that can offer images with a latency <200 ms, the offline reconstruction requires approximately 7 s per time frame. Machine learning algorithms[47,48] may have the potential to provide low-latency high-quality water/fat separated RT-MRI.

The proposed method is also robust to large off-resonance variation over space and time. In the abdomen example (Figure 5 and Video S5), gas bubbles within the bowel were present and moving, causing spatial and temporal variations in the off-resonance map that were detected, and did not compromise water/fat separation. We also pointed out in a representative short-axis slice of the heart (Video S6), the method was able to capture large temporal variations in off-resonance map with respiration.

This study has several limitations. One is that we did not perform systematic comparison of the proposed method with existing methods in all applications. Another limitation is we did not evaluate the proposed method in subjects with disorders for each application. This should be considered a demonstration of technical feasibility.

5 | CONCLUSIONS

We have demonstrated a novel and flexible bSSFP spiral OIOI pulse sequence and a two-step reconstruction at 0.55T that is able to provide water/fat separated RT-MRI. We demonstrated water/fat separated RT-MRI in the heart, wrist, and in the abdomen with a range of application-specific temporal resolution and spatial resolution requirements. The approach appears robust to large off-resonance variation over space and time.

ACKNOWLEDGMENTS

We acknowledge grant support from the National Science Foundation and National Institutes of Health, and research support from Siemens Healthineers. We also thank Skorn Ponrartana and Abhijit Chaudhari for helpful discussions.

FUNDING INFORMATION

National Science Foundation (#1828736). National Institutes of Health (R01-HL130494). National Institutes of Health (R21-HL159533). American Heart Association (903839).

DATA AVAILABILITY STATEMENT

We provide water-fat separated STCR reconstruction code, and one representative spiral OIOI RT-MRI raw dataset from each application at https://github.com/usc-mrel/spiral_oioi. Additional datasets will be made available upon reasonable request to the corresponding author.

ORCID

Ye Tian https://orcid.org/0000-0002-8559-4404

Krishna S. Nayak https://orcid.org/0000-0001-5735-3550

REFERENCES

1. Nayak KS, Lim Y, Campbell-Washburn AE, Steeden J. Real-Time Magnetic Resonance Imaging. *J Magn Reson Imaging*. 2022;55:81-99.
2. Campbell-Washburn AE, Tavallaei MA, Pop M, et al. Real-time MRI guidance of cardiac interventions. *J Magn Reson Imaging*. 2017;46:935-950.
3. Bhattacharya I, Ramasawmy R, Restivo MC, Campbell-Washburn AE. Dynamic speech imaging at 0.55T using single shot spirals for 11ms temporal resolution. In *Proceedings of the 27th Annual Meeting of ISMRM, Montreal, QC, Canada*; 2019:440.
4. Restivo MC, Ramasawmy R, Bandettini WP, Herzka DA, Campbell-Washburn AE. Efficient spiral in-out and

EPI balanced steady-state free precession cine imaging using a high-performance 0.55T MRI. *Magn Reson Med*. 2020;84:2364-2375.
5. Campbell-Washburn AE, Ramasawmy R, Restivo MC, et al. Opportunities in interventional and diagnostic imaging by using high-performance low-field-strength MRI. *Radiology*. 2019;293:384-393.
6. Borotikar B, Lempereur M, Lelievre M, Burdin V, Ben Salem D, Brochard S. Dynamic MRI to quantify musculoskeletal motion: a systematic review of concurrent validity and reliability, and perspectives for evaluation of musculoskeletal disorders. *PloS One*. 2017;12:e0189587.
7. Mazzoli V, Nederveen AJ, Oudeman J, et al. Water and fat separation in real-time MRI of joint movement with phase-sensitive bSSFP. *Magn Reson Med*. 2017;78:58-68.
8. de Jonge CS, Gollifer RM, Nederveen AJ, et al. Dynamic MRI for bowel motility imaging-how fast and how long? *Br J Radiol*. 2018;91:20170845.
9. Menys A, Taylor SA, Emmanuel A, et al. Global small bowel motility: assessment with dynamic MR imaging. *Radiology*. 2013;269:443-450.
10. Masselli G, Gualdi G. MR imaging of the small bowel. *Radiology*. 2012;264:333-348.
11. Meyer CH, Pauly JM, Macovski A, Nishimura DG. Simultaneous spatial and spectral selective excitation. *Magn Reson Med*. 1990;15:287-304.
12. Nayak KS, Cunningham CH, Santos JM, Pauly JM. Real-time cardiac MRI at 3 tesla. *Magn Reson Med*. 2004;51:655-660.
13. Delfaut EM, Beltran J, Johnson G, Rousseau J, Marchandise X, Cotten A. Fat suppression in MR imaging: techniques and pitfalls. *Radiographics*. 1999;19:373-382.
14. Tsao J, Jiang Y. Hierarchical IDEAL: fast, robust, and multiresolution separation of multiple chemical species from multiple echo times. *Magn Reson Med*. 2013;70:155-159.
15. Yu H, Reeder SB, Shimakawa A, Brittain JH, Pelc NJ. Field map estimation with a region growing scheme for iterative 3-point water-fat decomposition. *Magn Reson Med*. 2005;54:1032-1039.
16. Lu W, Hargreaves BA. Multiresolution field map estimation using golden section search for water-fat separation. *Magn Reson Med*. 2008;60:236-244.
17. Tan Z, Voit D, Kollmeier JM, Uecker M, Frahm J. Dynamic water/fat separation and B1 inhomogeneity mapping—joint estimation using undersampled triple-echo multi-spoke radial FLASH. *Magn Reson Med*. 2019;82:1000-1011.
18. Benkert T, Feng L, Sodickson DK, Chandarana H, Block KT. Free-breathing volumetric fat/water separation by combining radial sampling, compressed sensing, and parallel imaging. *Magn Reson Med*. 2017;78:565-576.
19. Hernando D, Kellman P, Haldar JP, Liang ZP. Robust water/fat separation in the presence of large field inhomogeneities using a graph cut algorithm. *Magn Reson Med*. 2010;63:79-90.
20. Lu A, Grist TM, Block WF. Fat/water separation in single acquisition steady-state free precession using multiple echo radial trajectories. *Magn Reson Med*. 2005;54:1051-1057.
21. Hargreaves B. https://mrsrl.stanford.edu/˜brian/vdspiral/
22. Pineda AR, Reeder SB, Wen Z, Pelc NJ. Cramér-Rao bounds for three-point decomposition of water and fat. *Magn Reson Med*. 2005;54:625-635.
23. Yu H, Shimakawa A, McKenzie CA, Brodsky E, Brittain JH, Reeder SB. Multiecho water-fat separation and simultaneous R2* estimation with multifrequency fat spectrum modeling. *Magn Reson Med*. 2008;60:1122-1134.
24. Nayak KS, Hargreaves BA, Hu BS, Nishimura DG, Pauly JM, Meyer CH. Spiral balanced steady-state free precession cardiac imaging. *Magn Reson Med*. 2005;53:1468-1473.
25. Feng L, Grimm R, Block KT, et al. Golden-angle radial sparse parallel MRI: combination of compressed sensing, parallel imaging, and golden-angle radial sampling for fast and flexible dynamic volumetric MRI. *Magn Reson Med*. 2014;72:707-717.
26. Winkelmann S, Schaeffter T, Koehler T, Eggers H, Doessel O. An optimal radial profile order based on the Golden ratio for time-resolved MRI. *IEEE Trans Med Imaging*. 2007;26:68-76.
27. Kim YC, Narayanan SS, Nayak KS. Flexible retrospective selection of temporal resolution in real-time speech MRI using a golden-ratio spiral view order. *Magn Reson Med*. 2011;65:1365-1371.
28. Tian Y, Lim Y, Zhao Z, Byrd D, Narayanan S, Nayak KS. Aliasing artifact reduction in spiral real-time MRI. *Magn Reson Med*. 2021;86:916-925.
29. Santos JM, Wright GA, Pauly JM. Flexible real-time magnetic resonance imaging framework. *Conf Proc IEEE Eng Med Biol Soc*. 2004;2004:1048-1051.
30. Adluru G, McGann C, Speier P, Kholmovski EG, Shaaban A, Dibella EV. Acquisition and reconstruction of undersampled radial data for myocardial perfusion magnetic resonance imaging. *J Magn Reson Imaging*. 2009;29:466-473.
31. Campbell-Washburn AE, Xue H, Lederman RJ, Faranesh AZ, Hansen MS. Real-time distortion correction of spiral and echo planar images using the gradient system impulse response function. *Magn Reson Med*. 2016;75:2278-2285.
32. Walsh DO, Gmitro AF, Marcellin MW. Adaptive reconstruction of phased array MR imagery. *Magn Reson Med*. 2000;43:682-690.
33. Lee NG, Ramasawmy R, Lim Y, Campbell-Washburn AE, Nayak KS. MaxGIRF: image reconstruction incorporating concomitant field and gradient impulse response function effects. *Magn Reson Med*. 2022;88:691-710.
34. King KF, Ganin A, Zhou XJ, Bernstein MA. Concomitant gradient field effects in spiral scans. *Magn Reson Med*. 1999;41:103-112.
35. Boutin RD, Buonocore MH, Immerman I, et al. Real-time magnetic resonance imaging (MRI) during active wrist motion – initial observations. *PloS One*. 2013;8:e84004.
36. Henrichon SS, Foster BH, Shaw C, et al. Dynamic MRI of the wrist in less than 20 seconds: normal midcarpal motion and reader reliability. *Skeletal Radiol*. 2020;49:241-248.
37. de Jonge CS, Smout AJPM, Nederveen AJ, Stoker J. Evaluation of gastrointestinal motility with MRI: advances, challenges and opportunities. *Neurogastroenterol Motil*. 2018;30:e13257.
38. Nayak KS. Response to letter to the editor: "nomenclature for real-time magnetic resonance imaging". *Magn Reson Med*. 2019;82:525-526.
39. Dixon WT. Simple proton spectroscopic imaging. *Radiology*. 1984;153:189-194.
40. Tasdelen B, Yagiz E, Cui SS, Nayak KS. *Ultra-Fast Water/Fat Imaging of the Abdomen at 0.55T*. In *Proceddings of ISMRM Workshop on Low Field MRI*; 2022 Virtual.
41. Fielden SW, Meyer CH. A simple acquisition strategy to avoid off-resonance blurring in spiral imaging with

redundant spiral-in/out k-space trajectories. *Magn Reson Med*. 2015;73:704-710.
42. Allen SP, Feng X, Fielden SW, Meyer CH. Correcting image blur in spiral, retraced in/out (RIO) acquisitions using a maximized energy objective. *Magn Reson Med*. 2019;81:1806-1817.
43. Schirda CV, Zhao T, Andronesi OC, et al. In vivo brain rosette spectroscopic imaging (RSI) with LASER excitation, constant gradient strength readout, and automated LCModel quantification for all voxels. *Magn Reson Med*. 2016;76:380-390.
44. Zhao Z, Lim Y, Byrd D, Narayanan S, Nayak KS. Improved 3D real-time MRI of speech production. *Magn Reson Med*. 2021;85:3182-3195.
45. Lim Y, Zhu Y, Lingala SG, Byrd D, Narayanan S, Nayak KS. 3D dynamic MRI of the vocal tract during natural speech. *Magn Reson Med*. 2019;81:1511-1520.
46. Bucholz EK, Song J, Johnson GA, Hancu I. Multispectral imaging with three-dimensional rosette trajectories. *Magn Reson Med*. 2008;59:581-589.
47. Lim Y, Bliesener Y, Narayanan S, Nayak KS. Deblurring for spiral real-time MRI using convolutional neural networks. *Magn Reson Med*. 2020;84:3438-3452.
48. Jafari R, Spincemaille P, Zhang J, et al. Deep neural network for water/fat separation: supervised training, unsupervised training, and no training. *Magn Reson Med*. 2021;85:2263-2277.

SUPPORTING INFORMATION

Additional supporting information may be found in the online version of the article at the publisher's website.

Table S1. Imaging parameters. Note that the FOV and temporal resolution during reconstruction are flexible due to the use of golden angle sampling and are not necessarily the same as the prescribed parameters from spiral trajectory design.

Figure S1. Impact of reconstruction temporal resolution. Image shows final water/fat separated RT images reconstructed with different temporal resolution: (top) 10.7 ms/frame, (middle) 42.8 ms/frame, and (bottom) 96.3 ms/frame. Images reconstructed with 10.7 ms/frame have residual artifacts (green arrow) and are unable to resolve fine structures like the papillary muscle in the right ventricle (yellow arrows). Movies reconstructed at 42.8 ms/frame and 96.3 ms/frame can capture the dynamics clearly for this volunteer, however, the 96.3 ms/frame reconstruction shows patchy structures in the time-line profiles (red arrows), suggesting it may not be enough for patients with higher heartrates or capturing irregular motion.

Figure S2. Comparison of water/fat separation without and with concomitant field phase correction. Shown is a representative two chamber long axis cardiac image processed without (top) and with (bottom) concomitant field phase correction. (A, B) time-averaged water/fat separation results without correction, (C) estimated off-resonance map without correction, and (D) time-averaged concomitant field phase. There is severe water/fat swap artifact in both the ROI (orange arrows) and outside the ROI (blue arrows). This is largely caused by the ambitious of estimating an off-resonance map with the effects from concomitant field, which has a large variation. As can be seen from the time-averaged concomitant field phase (D), the phase is larger as the location is further from the magnet iso-center, more likely to cause water/fat swapping. (E, F) show improved water/fat separation after the concomitant field phase correction and (G) shows off-resonance map with reduced variation caused by concomitant field.

Figure S3. Comparison of water/fat separated RT-MRI and Cartesian RT bSSFP of the small bowel. Images and intensity versus time plots are shown for one subject during free breathing, after drinking Breeza gastrointestinal contrast agent. The intensity vs. time profiles matches the blue dashed line. Note that (A) and (B) are also shown in Figure 5. The water-only image provides a clear depiction of the small bowel without the often-confounding presence of visceral adipose tissue signal. Small bowel motility can be evaluated during normal respiration (green arrows). The spiral OIOI water-only image has better temporal resolution and contrast than Cartesian images.

Figure S4. (A) Comparison of spiral OIOI fat-only image with the first spiral-out image in the wrist. The fat-only image has better contrast than the first spiral-out image, with ligament gaps being darker. The normalized line plots on the right show improved water-fat boundary contrast of the fat-only image. (B) comparison of spiral OIOI water-only image with the first spiral-out image in the heart. The image shows a zoomed-in 4-chamber view heart with a focus on the right coronary artery. The right coronary artery is clearly depicted in the water-only image, while it is surrounded by fat tissues without a clear boundary in the first spiral-out image. (C) comparison of spiral OIOI water-only image with first spiral-out image in the abdomen. The water-only image shows the small bowel clearer, while the first spiral-out image has a similar water and fat signal intensities and the small bowel is likely to be misidentified.

Video S1. Illustration of (left) online reconstruction and (mid and right) offline water/fat separated reconstruction. The volunteer was performing a radial-to-ulnar deviation maneuver, which is important in the evaluation of dynamic wrist instability. The online reconstruction is a gridding reconstruction that superimposes all the samples, giving a rough fat-only image. Online reconstruction has low latency (<200 ms) and coarse temporal resolution (1.3 frames/s), providing an initial inspection of image artifact and shimming performance. The offline reconstruction provides water and fat videos with high temporal resolution

(9.3 frames/s) and is insensitive to B_0 inhomogeneity, providing better visualization of the wrist anatomy and motion.

Video S2. Offline reconstructed RT images of all subjects ($N = 5$) underwent wrist scan. Video shows RT fat-only (left) and water-only (right) of each subject. In all subjects, the fat-only video has consistent high image quality to visualize the carpal bones movements and ligament gap deformations. The image quality for water-only video varies, mainly due to the low water component in the wrist and water being off resonance.

Video S3. Cardiac water/fat separated RT-MRI. One cardiac cycle of four-chamber view is shown from five volunteers. Water/fat videos obtained by spiral OIOI offer clear epicardial fat depiction and reveal detailed structures. The right coronary artery (blue arrows) and left circumflex artery (orange arrows) are clearly seen in the cross-section from the water images. The surrounding fat is also clearly visible in the fat images. Image artifacts are visible around the aorta, likely due to phase from the in-plane flow.

Video S4. Water/fat separated RT-MRI of the small bowel. A selected slice was shown from one subject during free breathing, after drinking Breeza gastrointestinal contrast agent. Video is displayed at normal speed in the beginning and at 5 times accelerated speed in the end to better illustrate the motion. The water-only video provides a clear depiction of the small bowel without the often-confounding presence of visceral adipose tissue signal. Small bowel motility can be evaluated during normal respiration.

Video S5. Water/fat separated RT-MRI in all subjects ($N = 3$) underwent abdominal scan. Video shows 7–8 slices from each subject that small bowel movements are clearly seen. Video is displayed at 5 times acceleration to better visualize the motion. Consistent high quality and high contrast was seen on the spiral OIOI water-only videos. Air bubbles also presented in some slices without causing significant imaging artifacts.

Video S6. Water/fat separated RT-MRI and dynamic field map of the heart. A mid short-axis view of the heart is shown with water-only video, fat-only video, and dynamic off-resonance map at the top and time-line profiles at the bottom. The data was acquired without breath-hold as significant breathing motion can be seen. The estimated dynamic off-resonance map was able to capture this motion and offer motioned resolved water-only and fat-only videos.

How to cite this article: Tian Y, Nayak KS. Real-time water/fat imaging at 0.55T with spiral out-in-out-in sampling. *Magn Reson Med*. 2024;91:649-659. doi: 10.1002/mrm.29885